AD-A150 752 THE DOWNSHIFT OF ELECTRON PLASMA OSCILLATIONS IN THE ELECTRON FORESHOCK R.. (U) IOWA UNIV IOWA CITY DEPT OF PHYSICS AND ASTRONOMY S A FUSELIER ET AL. 10 OCT 84 1/1

UNCLASSIFIED U. OF IOWA-84-21 N00014-76-C-0016 F/G 20/9 NL

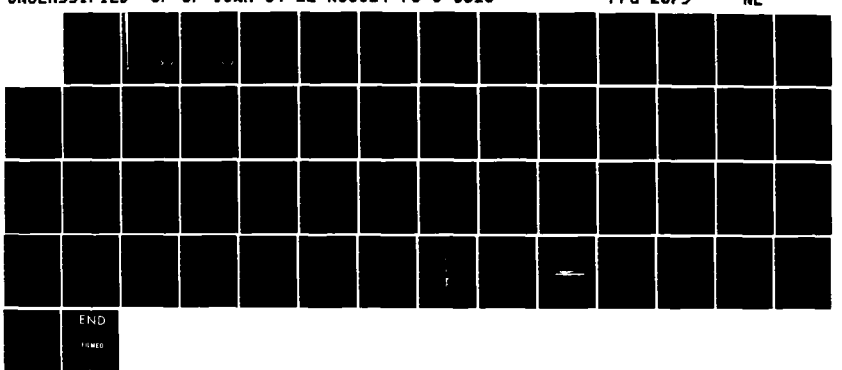

END

FILMED

DTIC

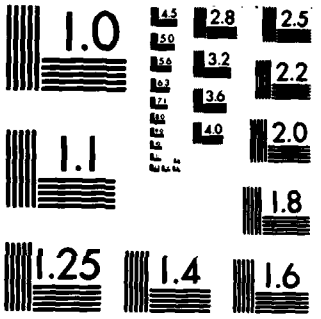

U. of Iowa 84-21

(1)

THE DOWNSHIFT OF ELECTRON PLASMA OSCILLATIONS IN THE ELECTRON FORESHOCK REGION

by

S. A. Fuselier[1], D. A. Gurnett[1],

and R. J. Fitzenreiter[2]

Department of Physics and Astronomy

THE UNIVERSITY OF IOWA

Iowa City, Iowa 52242

U. of Iowa 84-21

THE DOWNSHIFT OF ELECTRON PLASMA OSCILLATIONS IN THE ELECTRON FORESHOCK REGION

by

S. A. Fuselier[1], D. A. Gurnett[1],

and R. J. Fitzenreiter[2]

April 1984

[1] Department of Physics and Astronomy
The University of Iowa
Iowa City, I. 52242

[2] Goddard Space Flight Center
Greenbelt, MD 20771

The research at the University of Iowa was supported by contract NAS5-26819 with Goddard Space Flight Center, grant NGL-16-001-043 with NASA Headquarters, and grant N00014-76-C-0016 with the Office of Naval Research.

UNCLASSIFIED

SECURITY CLASSIFICATION OF THIS PAGE (When Data Entered)

REPORT DOCUMENTATION PAGE	READ INSTRUCTIONS BEFORE COMPLETING FORM
1. REPORT NUMBER: U. of Iowa-84-21	2. GOVT ACCESSION NO.: AD-A150 752
3. RECIPIENT'S CATALOG NUMBER	
4. TITLE (and Subtitle): THE DOWNSHIFT OF ELECTRON PLASMA OSCILLATIONS IN THE ELECTRON FORESHOCK REGION	5. TYPE OF REPORT & PERIOD COVERED: Progress October 1984
	6. PERFORMING ORG. REPORT NUMBER
7. AUTHOR(s): S. A. FUSELIER, D. A. GURNETT, and R. J. FITZENREITER	8. CONTRACT OR GRANT NUMBER(s): N00014-76-C-0016
9. PERFORMING ORGANIZATION NAME AND ADDRESS: Department of Physics and Astronomy, University of Iowa, Iowa City, Iowa 52242	10. PROGRAM ELEMENT, PROJECT, TASK AREA & WORK UNIT NUMBERS
11. CONTROLLING OFFICE NAME AND ADDRESS: Electronics Program Office, Office of Naval Research, Arlington, VA 22217	12. REPORT DATE: 10 October 1984
	13. NUMBER OF PAGES: 53
14. MONITORING AGENCY NAME & ADDRESS (if different from Controlling Office)	15. SECURITY CLASS. (of this report): Unclassified
	15a. DECLASSIFICATION/DOWNGRADING SCHEDULE

16. DISTRIBUTION STATEMENT (of this Report)

Approved for public release; distribution is unlimited.

17. DISTRIBUTION STATEMENT (of the abstract entered in Block 20, if different from Report)

18. SUPPLEMENTARY NOTES

To be published in Journal of Geophysical Research, March, 1985.

19. KEY WORDS (Continue on reverse side if necessary and identify by block number)

Plasma oscillations, Langmuir waves, foreshock.

from p. 2

20. ABSTRACT (Continue on reverse side if necessary and identify by block number)

See following page.

DD FORM 1 JAN 73 1473 EDITION OF 1 NOV 65 IS OBSOLETE
S/N 0102-LF-014-6601

UNCLASSIFIED

SECURITY CLASSIFICATION OF THIS PAGE (When Data Entered)

ABSTRACT

Electron plasma oscillations in the Earth's electron foreshock region are observed to shift above and below the local electron plasma frequency. As plasma oscillations shift downward from the plasma frequency, their bandwidth increases and their wavelength decreases. Observations of plasma oscillations well below the plasma frequency are correlated with times when ISEE-1 is far downstream of the electron foreshock boundary. Although wavelengths of plasma oscillations below the plasma frequency satisfy $k\lambda_{De} \approx 1$, the Doppler-shift due to the motion of the solar wind is not sufficient to produce the observed frequency shifts. A beam-plasma interaction with beam velocities on the order of the electron thermal velocity is suggested as an explanation for plasma oscillations above and below the plasma frequency. Frequency, bandwidth, and wavelength changes predicted from the beam-plasma interaction are in good agreement with the observed characteristics of plasma oscillations in the foreshock region.

Originator-supplied keywords included. → p. 1473

INTRODUCTION

In this paper, observations of electron plasma oscillations are interpreted using a beam-plasma theory. Electron plasma oscillations upstream of the Earth's bow shock were first reported by Fredricks et al. [1968]. Using OGO-5 spacecraft data, they reported enhanced electric field intensities near the local electron plasma frequency. Also using OGO-5 spacecraft data, Scarf et al. [1971] identified electric field enhancements near the local plasma frequency and associated these enhancements with electrons streaming into the solar wind from the bow shock. The waves were identified by Scarf et al. as either electron plasma oscillations or upper hybrid waves. Later, Fredricks et al. [1971] demonstrated that observations of electric field enhancements near the plasma frequency were consistent with the interpretation that the waves were electron plasma oscillations generated by a beam-plasma interaction. The electrostatic nature of the waves was confirmed by Rodriguez and Gurnett [1975], using simultaneous electric and magnetic field measurements from IMP-6.

Following the observations of the emissions at the plasma frequency, their polarization and wavelength were measured by several investigators. The polarization of the oscillations was measured from IMP-6 data by Rodriguez and Gurnett [1975, 1976], and was found to be primarily along the magnetic field. This measurement confirmed the identification of the waves as electron plasma oscillations, and

eliminated the possibility that they are upper hybrid waves. The wavelength of the plasma oscillations was estimated to be several kilometers by Gurnett and Frank [1975]. These wavelength estimates were confirmed by Gurnett et al. [1979] and Anderson et al. [1981], using ISEE-1 and -2 electric field data.

Filbert and Kellogg [1979] were the first to consider the detailed origin of the electron beams responsible for the plasma oscillations. They analyzed the effect of the motion of the solar wind on electrons streaming from the bow shock. Electrons streaming from the bow shock are convected downstream due to the $\vec{v} \times \vec{B}$ electric field of the solar wind. As illustrated in Figure 1, high energy electrons originating from the tangent point define a boundary called the electron foreshock boundary. Upstream of this boundary, no electrons streaming from the bow shock are observed. The region downstream of the foreshock boundary and upstream of the bow shock is called the electron foreshock region. Filbert and Kellogg noted that electrons streaming into the solar wind from the bow shock with velocities below a certain critical velocity can not reach the spacecraft. The magnitude of the critical velocity depends on the location of the spacecraft in the foreshock region. In the foreshock region, the reduced one dimensional electron distribution in the plasma rest frame has a positive slope at the critical velocity. This reduced electron distribution is called a time-of-flight distribution. Filbert and Kellogg considered a model time-of-flight distribution with the critical velocity much greater than the electron thermal velocity and demonstrated that plasma oscillations can be generated near the electron plasma frequency. This

model is valid for times when the spacecraft is located near the foreshock boundary. Intense electrostatic emissions at the plasma frequency were reported by Filbert and Kellogg coincident with foreshock boundary crossings. They suggested that high energy electron beams, of the type first reported by Anderson [1968, 1969], should be coincident with foreshock boundary crossings. Thin sheets of high energy electrons associated with the foreshock boundary were reported by Anderson et al. [1979]. Also, reduced distributions associated with the foreshock boundary have been reported by Fitzenreiter et al. [1984] which may be unstable to generation of electron plasma oscillations.

Another feature of plasma oscillations in the foreshock region is that they are observed to vary in frequency. Frequency variations of plasma oscillations on the order of a few kHz were reported by Fredricks et al. [1972]. These frequency variations were correlated with fluctuations in both the local electron density and the total magnetic field. Based on the magnetic field fluctuations, it was suggested by Fredricks et al. that these frequency variations were caused by electron density fluctuations associated with oblique magnetohydrodynamic waves in the foreshock region.

A different type of frequency variation of the electrostatic emissions in the foreshock region was reported by Rodriguez and Gurnett [1975]. They reported observations of electrostatic emissions from 3 kHz to the plasma frequency, which is usually about 30 kHz. It is not clear from their study which electrostatic wave mode was observed below the plasma frequency. The emissions observed could have been a mixture of ion acoustic waves, which range from 0 to 10 kHz, and electron

plasma oscillations, which as will be shown, range from near 0 kHz to about 30 kHz. It was suggested by Rodriguez and Gurnett that the emissions below the plasma frequency were plasma oscillations that were strongly Doppler shifted due to the motion of the solar wind. However, their explanation is doubtful because if the wavelength at the plasma frequency is several kilometers, as estimated by Gurnett and Frank [1975], then the Doppler shift due to the motion of the solar wind is less than 1 kHz.

Recently, Etcheto and Faucheux [1984] made a detailed study of the plasma oscillations below the plasma frequency, using data from the relaxation sounder [Harvey et al., 1978] on ISEE-1. They reported plasma oscillations not only below the plasma frequency, but also slightly above the plasma frequency. The plasma oscillations below the plasma frequency were reported to have large bandwidths ($\Delta f/f \simeq 0.3$) and long wavelengths ($\lambda >> \lambda_{De}$). The observations of plasma oscillations below the plasma frequency were also found to be correlated with times where ISEE-1 was far downstream of the foreshock boundary. The mechanism for generation of plasma oscillations below the plasma frequency was not identified.

The purpose of this paper is, first, to report high-time resolution observations of plasma oscillations at, above, and below the plasma frequency, second, to discuss the characteristics of the plasma oscillations, and third, to propose a mechanism for explaining the shift in the frequency of the oscillations away from the plasma frequency. High-resolution spectrograms from the University of Iowa wideband receiver on ISEE-1 are used to study the complex temporal and

frequency structure of the plasma oscillations below the plasma frequency. Some of the characteristics are found to differ from those reported by Etcheto and Faucheux [1984]. Predictions from the proposed mechanism are found to agree with the observed frequency shift, bandwidth, and wavelength presented in this paper.

Plasma wave data from the University of Iowa plasma wave instruments on ISEE-1 and -2 are used in this study. A description of the plasma wave instruments is given by Gurnett et al. [1978]. Density, solar wind velocity, and temperature values in this study are a result of moment calculations of three dimensional distributions measured by the Goddard Space Flight Center electron spectrometer on ISEE-1. For information on the Goddard Space Flight Center electron spectrometer, see Ogilvie et al. [1978]. In addition to moments of the electron distribution, the time evolution of the reduced one dimensional electron distribution, $F(v_{\parallel})$ is used in this study.

OBSERVATIONS OF PLASMA OSCILLATIONS

Electron plasma oscillations in the electron foreshock region occur at the local plasma frequency, and in some cases may shift slightly above or substantially below the plasma frequency. Plasma oscillations are observed at frequencies ranging from less than 0.1 f_{pe} to about 1.1 f_{pe}, where f_{pe} is the local electron plasma frequency, ($f_{pe} = 9000\sqrt{n_o}$ Hz). For the foreshock region, this frequency range is from about 3 to 30 kHz. A typical example of plasma oscillations that are shifted substantially from the plasma frequency is illustrated in Figure 2. The upper panel of Figure 2 is a wideband frequency-time spectrogram from the ISEE-1 wideband receiver which was taken when the spacecraft was located in the foreshock region. In the lower panel of Figure 2, the plasma frequency was calculated from the equation $f_{pe} = 9000\sqrt{n_o}$, where n_o is the electron density in units of cm^{-3}, and the frequency is in Hz. During the time interval from 0633:00 UT to 0633:30 UT, the plasma oscillations are seen to vary from f_{pe} to about .25 f_{pe}.

The complex nature of the plasma oscillations illustrated in Figure 2 is due to the presence of MHD waves associated with ions streaming from the bow shock [Scarf et al., 1970]. The presence of MHD waves is inferred from the fluctuations in the electron density. The presence of the ions streaming from the bow shock is inferred from the presence of ion acoustic waves in the 0-10 kHz range. The effects of the MHD

waves on the frequency spectrum is not considered in this study because, as will be shown, the downshifts of plasma oscillations also occur when the MHD waves and upstreaming ions are not present.

Another characteristic of plasma oscillations, which was discussed by Etcheto and Faucheux [1984], is illustrated in Figure 2. At 0638:40 UT, the plasma oscillations appear as a narrowband emission near the plasma frequency. From 0638:40 UT to 0639 UT, the plasma oscillations shift downward from the plasma frequency. Coincident with this shift, the bandwidth of the emissions increases from a few hundred Hz to about ±2 kHz. From the study of numerous events such as those illustrated in Figure 2, it was found that an increase in the bandwidth of plasma oscillations always accompanies a large shift in the frequency away from the plasma frequency.

In addition to the change in the bandwidth, the wavelength of plasma oscillations below the plasma frequency also changes. The wavelength of electrostatic emissions such as plasma oscillations can be infered by comparing spectral density measurements obtained from two different length electric antennas. To obtain the wavelengths of plasma oscillations at the plasma frequency, Gurnett et al. [1979] compared spectral density measurments from a 215 meter dipole antenna on ISEE-1 to measurements from a 30 meter dipole antenna on ISEE-2. It was found that spectral density measurements at the plasma frequency from the two antenna agreed within 10%. Gurnett et al. concluded that plasma oscillations at the plasma frequency have wavelengths longer than the antenna on ISEE-1. A typical electron Debye length in the foreshock region is 9 meters, so plasma oscillations at the plasma

frequency satisfy the relation, $k\lambda_{De} << 1$. The long wavelengths of plasma oscillations observed at the plasma frequency were also verified by Anderson et al. [1981] using the same method.

In this study, electric field spectrums obtained from ISEE-1 plasma wave data are compared to ISEE-2 for times when plasma oscillations are observed to shift well below the plasma frequency. Spectrums from over 15 hours of data containing downshift events were compared. An example of this comparison is illustrated in Figure 3. The electric field spectrums were averaged over 20 minutes to obtain the graph illustrated in Figure 3. The time interval in Figure 3 contained numerous downshift events similar to those illustrated in Figure 2. During the 20-minute interval the spacecraft were 30 km apart and both spacecraft were moving at about 1 km/sec. The long averaging time and the close proximity of ISEE-1 to ISEE-2 were chosen to reduce temporal and spatial aliasing of the separate measurements of the spectral density. For frequencies between 10 kHz and 20 kHz, the spectral densities measured by ISEE-2 are greater than those measured by ISEE-1 by about a factor of 5. At the local plasma frequency (30 kHz), the spectral density measurements from the two spacecraft differ by less than 10%. The difference in the measured spectral densities for frequencies between 10 kHz and 20 kHz is interpreted as an indication that the wavelengths of plasma oscillations below the plasma frequency are between 30 and 215 meters. Since a typical Debye length for the foreshock region is about 9 meters, wavelengths between 30 and 215 meters satisfy $k\lambda_{De} \approx 1$. As a result of the study of numerous spectral density comparisons similar to the one illustrated in Figure 3, it is

concluded that when the frequency is shifted well below the plasma frequency, plasma oscillations have short wavelengths, $\lambda \approx 2\pi\lambda_{De}$, and when the frequency is at the plasma frequency, plasma oscillations have long wavelengths, $\lambda >> \lambda_{De}$. The wavelength is assumed to decrease in a continuous manner because plasma oscillations shift in a continuous manner from the plasma frequency to well below the plasma frequency.

In contrast to the report in this paper of short wavelengths below the plasma frequency, Etcheto and Faucheux [1984] report long wavelengths below the plasma frequency. Etcheto and Faucheux found no difference in the spectral density measurements from the 215 meter long wire dipole antenna on ISEE-1 and the 130 meter sphere-to-sphere antenna, also on ISEE-1. The small difference in the effective lengths of the two antennas (at best a factor of 2) may account for the fact that no difference in the two spectral density measurements was observed. In contrast, the difference in the spectral density measurements in Figure 3 of this paper is distinguishable because the effective lengths of the two dipole antennas used in the comparison differ by about a factor of 7. Thus, the smaller difference in the effective lengths of the two antennas used by Etcheto and Faucheux may account for the fact that no difference in the spectral density measurements below the plasma frequency was observed and thus it was concluded that the wavelengths were long.

Although plasma oscillations below the plasma frequency are reported in this paper to have short wavelengths, the observed shifts from the plasma frequency can not be attributed entirely to Doppler-shifts. Consider for example, the event illustrated in Figure 2. On

October 31, 1977, at 0633 UT, the solar wind velocity was 335 km/second, the number density was 5 cm^{-3} and the electron temperature was 1.1×10^5K. Assuming plasma oscillations with a minimum wavelength of $2\pi\lambda_{De}$, the maximum Doppler shift is estimated to be 5 kHz. The maximum Doppler shift is only about 50% of the observed shift from the plasma frequency in Figure 2. For example, at 0638:50 UT, plasma oscillations are observed at .33 f_{pe}, but plasma oscillations Doppler-shifted from the plasma frequency would occur at or above .7 f_{pe}.

A study was performed to determine the change in the characteristics of both the wave and particle data as ISEE-1 penetrates deeper into the foreshock region. This study was similar to that of Etcheto and Faucheux [1984]. The three-dimensional model of the bow shock used in the study is discussed by Filbert and Kellogg [1979]. The equation for the bow shock is,

$$X = 14.6 - 0.0223\ (Y^2 + Z^2) \qquad (1)$$

where X, Y, and Z are the geocentric solar ecliptic (GSE) coordinates of the bow shock in units of Earth radii. ISEE-1 data pool values for spacecraft coordinates and magnetic field components were used. The solar wind flow velocity was assumed to be in the $-X_{GSE}$ direction. If the magnetic field was found to intersect the bow shock, then the distance along the solar wind velocity from the tangent field line to the spacecraft field line was computed. This distance is an indication of the depth of penetration of the spacecraft into the foreshock region. The simple bow shock model and 64 second average magnetic field data is

adequate for the study because large uncertainties in the shape and location of the bow shock and rapid changes in the magnetic field geometry allows only a qualitative discussion of the spacecraft location. In this study, 25 hours of wideband data containing over 150 foreshock boundary crossings were used. These events covered a wide range of magnetic field geometries and spacecraft locations.

The characteristics of plasma oscillations were found to depend on the depth of penetration of the spacecraft into the foreshock region. An example of the change in characteristics of plasma oscillations is illustrated in the middle and lower panels of Figure 4. The middle panel of Figure 4 is a frequency-time spectrogram from ISEE-1. In the middle panel, the narrowband emissions at 18 kHz are electron plasma oscillations. The lower panel is a plot of Diff. A large, negative value of Diff implies that the spacecraft is far downstream of the foreshock boundary. A positive value of Diff implies that the spacecraft is on a field line not connected to the bow shock. From 1237 to 1238 UT, the spacecraft moves from the foreshock boundary to a few R_E downstream of the foreshock boundary and plasma oscillations shift from the plasma frequency to slightly above the plasma frequency. From 1238 to 1240:30 UT, the spacecraft moves from a few R_E downstream of the foreshock boundary to far downstream of the foreshock boundary. Coincident with this movement, plasma oscillations shift from slightly above the plasma frequency to well below the plasma frequency. From 1241:30 to 1242:30 UT, the spacecraft moves from far downstream of the foreshock boundary to just upstream of the foreshock boundary. Coincident with this movement, plasma oscillations shift first from

well below the plasma frequency to slightly above the plasma frequency, then from slightly above the plasma frequency to the plasma frequency.

There is a considerable difference between the spectrum in the middle panel of Figure 4 and the spectrum in Figure 2. The reason for this difference is that ISEE-1 is upstream of the ion foreshock boundary during the event illustrated in Figure 4 and is downstream of the ion foreshock boundary during the event illustrated in Figure 2. The lack of ion acoustic waves in the 0-10 kHz range in the spectrogram in Figure 4 is an indication that there are no upstreaming ions present. (The dark band in the 0-10 kHz range is an artifact of the processing of the wideband data and is not ion acoustic waves.) Because downshifts of plasma oscillations occur when no upstreaming ions are present, it is concluded that the downshifts are not generated by presence of ion beams.

The differences in the spectrograms illustrated in Figures 2 and 4 would be difficult to distinguish using a sounding instrument such as that used in the study by Etcheto and Faucheux [1984]. The reason for this difficulty is that the sweep time for the sounder (16 sec for 0-50 kHz) is slow enough that discrete features, such as those illustrated in Figure 2, would not appear in the spectrogram. The result would be that one would almost always observe a spectra similar to that in the middle panel of Figure 4. Thus, using the high time resolution ($\Delta t \approx$ 50 milliseconds) wideband data, a fourth classification of plasma oscillations in the foreshock region is identified. The first three classifications of plasma oscillations in the foreshock region were identified by Etcheto and Faucheux [1984] as narrowband emissions at

the plasma frequency, broadband emissions slightly above the plasma frequency, and broadband emissions below the plasma frequency. The fourth classification, illustrated in Figure 2, is identifiable by complex, discrete fluctuations of plasma oscillations and is associated with times when the spacecraft is downstream of both the electron and the ion foreshock boundary. These classifications are somewhat arbitrary because plasma oscillations change continuously from one to the other as the spacecraft moves from near the electron foreshock boundary to far downstream of the foreshock boundary.

The change in the characteristics of plasma oscillations is not only associated with deeper penetration into the foreshock region, but is also associated with changes in the electron spectra. Comparison of wave data and electron data from the Goddard Space Flight Center electron spectrometer for over 50 foreshock boundary crossings was made. The electron spectrometer was chosen for this study because this instrument can detect the electrons responsible for generation of plasma oscillations and reduced one-dimensional distributions can be generated from the electron data.

A good correlation was observed between the shift of plasma oscillations from the plasma frequency and the increase in the flux of energetic electrons at successively lower velocities. One example of this correlation is illustrated in the upper and middle panels of Figure 4. The upper panel of Figure 4 is a plot of iso-contours of constant $-\ell n(F(v_{\parallel}))$ for electrons propagating upstream from the bow shock. Here, $F(v_{\parallel})$ is defined as the reduced distribution function. Each contour represents a change of a factor of $\ell n(e)$. The phase space density

decreases with increasing velocity. The electron thermal velocity is about 1500 km/sec. A shift of a contour from low to high parallel velocities is an indication of an increase in the flux of electrons. For example, from 1237 - 1238 UT, the contour at 10,000 km/sec shifts to about 12,000 km/sec, indicating an increase in the flux of electrons with velocities equal to 10,000 km/sec. The middle panel is a frequency-time spectrogram.

From 1237:15 to 1239 UT, Diff changes from about -5 R_E to -60 R_E, indicating that the location of ISEE-1 in the foreshock region changes from near the foreshock boundary to far downstream of the foreshock boundary. Coincident with the change of location in the foreshock region, plasma oscillations shift upward to about 1.1 f_{pe}, and then downward to about .7 f_{pe}. As the plasma oscillations shift downward in frequency, the flux of energetic electrons arriving from the bow shock increases at successively lower velocities from 1237:15 to 1239 UT. This trend is illustrated by the first dashed line in the upper panel of Figure 4. From 1240:30 to 1242 UT, Diff changes from about -120 R_E to -5 R_E, indicating that the location of ISEE-1 in the foreshock region changes from far downstream of the foreshock boundary to near the foreshock boundary. The change in the location is accompanied by a shift of the frequency of plasma oscillations from about .6 f_{pe} to 1.0 f_{pe}. The change in the location is also accompanied by a decrease in the flux of energetic electrons at successively higher velocities, as illustrated by the second dashed line in the upper panel of Figure 4. From 1242 to 1244 UT, ISEE-1 is on a magnetic field line which may not be connected to the bow shock. There is no evidence of electrons from

the bow shock with velocities less than 30,000 km/sec in the electron data. The emissions observed at the plasma frequency from 1242 to 1244 UT may be generated by electrons from the bow shock with velocities greater than 30,000 km/sec or may be enhanced thermal emissions [Hoang et al., 1980]. The intensity of these emissions is four orders of magnitude lower than plasma oscillations that are associated with electrons from the bow shock at 1241 UT. There is no change in the apparent intensity of the emissions in the frequency-time spectrogram because of an automatic gain control on the wideband receiver.

The correlation between the increase in flux of energetic electrons at successively lower velocities and the deeper penetration of the spacecraft into the foreshock region may be an indication that the time-of-flight mechanism discussed by Filbert and Kellogg has an effect on the electron distribution from velocities much greater than the electron thermal velocity to velocities on the order of the electron thermal velocity. This effect is illustrated in Figure 5. When ISEE-1 is far downstream of the foreshock boundary (Figure 5, case 1), the critical velocity may be on the order of the electron thermal velocity. When ISEE-1 is near the the foreshock boundary (Figure 5, case 2), the critical velocity is much greater than the electron thermal velocity.

A study of the electron data for several foreshock boundary crossings was made to determine if unstable distributions of the type reported by Fitzenreiter et al. [1984] are observed throughout the foreshock region. Reduced one-dimensional distributions that may be unstable to generation of plasma oscillations were found for times when ISEE-1 was located near the foreshock boundary. As the spacecraft

penetrated deeper into the foreshock region, the reduced distribution was observed to evolve from a double-peaked distribution to a single-peaked distribution. An example of the time evolution of a reduced distribution is illustrated in Figure 6. The upper part of Figure 6, shows three reduced distributions generated from data taken over 3-second intervals spaced 18 seconds apart. A reference solar wind distribution observed where the spacecraft was not connected to the bow shock is also shown with three reduced distributions. In the lower part of Figure 6, a frequency-time spectrogram and a plot of Diff are illustrated. From 1237:16 to 1238:20 UT, Diff changed from -5.6 R_E to -19.0 R_E, indicating that ISEE-1 penetrated deeper into the electron foreshock region. Coincident with this time period, at 1237:51 UT a second peak with a number density of about 10^{-3} - 10^{-4} n_o and a parallel velocity of about 9,500 km/sec is observed in the reduced distribution. In the second distribution, at 1238:09 UT, a plateau at a parallel velocity of about 6,000 km/sec is observed in the reduced distribution. At 1238:27.6 UT, when ISEE-1 is about 25 R_E downstream of the foreshock boundary and plasma oscillations occur below the plasma frequency, there is no second peak or plateau visible in the reduced distribution.

A simulation of another event similar to the one discussed above was made to determine if the electron spectrometer could detect a low density beam at velocities on the order of the electron thermal velocity. In the simulation, the instrument's velocity space sampling was used to sample a model plasma and beam distribution. It was found that a beam with $n_b = 10^{-2} - 10^{-3}$ n_o could be detected for any beam

velocity, provided that the beam remained at a fixed velocity for the 3 seconds used to generate a reduced distribution. Reduced distributions can be generated from less than 3 seconds of data, however, coverage of velocity space is reduced and the chances of detecting beams are diminished.

From the study of wideband data similar to that shown in Figure 6, there are indications that plasma oscillations below the plasma frequency may be generated by a beam whose velocity varies significantly over a 3-second time period. Inspection of wideband spectrograms reveals that plasma oscillations below the plasma frequency are time varying emissions spread over a broad range of frequencies. Typically, bursts of less than 50 milliseconds separated by a few tens of milliseconds, are observed. The bandwidths of these bursts are usually about 5 kHz. When these bursts are illustrated in a compressed time format as in Figure 4, they appear continuous. When the time scale is expanded as in Figure 6, at 1238:20 - 1238:35 UT, plasma oscillations below the plasma frequency are bursts of short duration which vary in frequency. It will be shown in the next sections that, in the context of linear plasma theory, the temporal and frequency variations of plasma oscillations below the plasma frequency are consistent with the interpretation that plasma oscillations are generated by a beam that varies significantly in velocity on time scales of a few tens of milliseconds. These time scales are much too short to be resolved by any existing electron detector.

Before considering a mechanism for generation of plasma oscillations at, somewhat above, and much below the plasma frequency, a summary of the basic characteristics of plasma oscillations in the foreshock region is given below.

1. Plasma oscillations are observed at frequencies ranging from less than 0.1 f_{pe} to about 1.1 f_{pe}.
2. As the plasma oscillations shift below the plasma frequency, their bandwidth increases from a few hundred hertz near the plasma frequency to ±2 kHz well below the plasma frequency.
3. Plasma oscillations at the plasma frequency have wavelengths much greater than a Debye length. Plasma oscillations at frequencies well below the plasma frequency have wavelengths on the order of a few Debye lengths.
4. Plasma oscillations much below the plasma frequency are correlated with times when ISEE-1 is located deep in the foreshock region, far downstream of the foreshock boundary.
5. As the plasma oscillations shift below the plasma frequency, the flux of energetic electrons streaming from the bow shock increases at successively lower velocities.

BEAM-PLASMA THEORY

As discussed in the introduction, a mechanism for producing unstable electron distribution functions was demonstrated by Filbert and Kellogg [1979]. They considered an electron distribution at times when a spacecraft is located near the foreshock boundary. For these times, the critical velocity of the beam is much greater than the electron thermal velocity. Downstream of the foreshock boundary, the critical velocity of the beam approaches the electron thermal velocity. To obtain solutions of the linear dispersion relation valid for the entire foreshock region, one must consider a beam-plasma interaction without the restriction that the beam velocity be much greater than the electron thermal velocity. Briggs [1964], Reinleitner et al. [1983], and Grabbe [1984], have considered approximations to the linear dispersion relation and have obtained analytical solutions for $\omega(k)$. In this paper, a numerical solution to the dispersion relation for a plasma and an electron beam will be presented. Solutions to the dispersion relation are obtained for all beam velocities.

Solution of the linear Vlasov equation yields a dispersion relation of the form,

$$D(k,\omega) = 0 = 1 - \sum_s \frac{\omega_{ps}^2}{k^2} \int \frac{\partial F_{os}(v_z)/\partial v_z}{v_z - \frac{\omega}{k}} dv_z \qquad (2)$$

where ω_{ps} is the plasma frequency of the s^{th} species, k is the wave number, $F_{os}(v_z)$ is the reduced one dimensional distribution function for the s^{th} species, and ω is the complex frequency.

The electron distribution in the foreshock region is approximated by a Maxwellian distribution,

$$F_{oe}(v_z) = \left[\frac{1}{2\pi V_t^2}\right]^{1/2} e^{-[v_z^2/2V_t^2]} \tag{3}$$

where V_t is the electron thermal velocity. The electron distribution in the foreshock is more closely approximated by a bi-Maxwellian [Feldman et al., 1975]. However, the results presented below using a single Maxwellian do not differ greatly from the results obtained using a bi-Maxwellian. The electron beam is approximated by a Lorentzian distribution,

$$F_{ob}(v_z) = \frac{C_b}{\pi} \frac{1}{C_b^2 + (v_z - V_b)^2} \tag{4}$$

where C_b is the thermal velocity of the beam and V_b is the beam velocity. Ions are neglected because the downshifts of plasma oscillations occur when there are no ions observed streaming from the bow shock and because the solar wind ion distribution has a negligible effect on the solutions of dispersion relation.

Substituting Equation 3 and Equation 4 into Equation 2 and integrating one finds,

$$D(k,\omega) = 0 = 1 + (k\lambda_{De})^2 + zZ(z) - \frac{n_b/n_o(k\lambda_{De})^2}{(k\lambda_{De}V_b/V_t - ik\lambda_{De}T_b/T_e - \omega/\omega_{pe})^2} . \quad (5)$$

Where n_b and n_o are the number density of the beam and the plasma, respectively, T_b and T_e are the temperatures of the beam and the plasma, respectively, $Z = \omega/kV_t\sqrt{2}$, and $Z(z)$ is the plasma dispersion function [Fried and Conte, 1961].

Equation 5 can be solved for $\omega(k)$ numerically using the Muller method [Muller, 1956]. An example of solutions of Equation 5 is illustrated in Figure 7. This illustration shows a graph of ω_i/ω_{pe} versus ω_r/ω_{pe} for $T_b/T_e = 0$, $n_b/n_o = 0.01$, and $V_b/V_t = 0.5$, 1.0, 2.0, 2.5, and 3.0, where ω_i is the growth rate and ω_r is the frequency.

For $T_b/T_e \neq 0$, the growth rate for specific values of V_b/V_t is less than the growth rate for $T_b/T_e = 0$. If T_b/T_e is large enough, solutions of the dispersion relation for some values of V_b/V_t are Landau damped. For example, if $T_b/T_e = 0.05$, plasma oscillations are damped for $V_b/V_t < 0.9$ and the maximum growth rate for $V_b/V_t = 1.5$ has decreased by a factor of 3 from the growth rate for $V_b/V_t = 1.5$ and $T_b/T_e = 0$. The reduced growth rate for frequencies below the plasma frequency will not be reflected in the observations if the waves have sufficient time to grow beyond the small amplitude approximation made in the linear Vlasov theory. A non-linear saturation of the signal would account for the constant spectral density from 0.3 f_{pe} to f_{pe} in Figure 3.

For specific values of V_b/V_t, T_b/T_e, and n_b/n_o, the frequency with the largest growth rate will be the observed frequency. Figure 8 shows the frequency of maximum growth versus V_b/V_t, for $n_b/n_o = 0.01$ and $T_b/T_e = 0$, 0.005, 0.01, 0.05, and 0.1. The wave number of maximum growth versus V_b/V_t for the same values of n_b/n_o and T_b/T_e is illustrated in Figure 9.

The values of n_b/n_o and T_b/T_e were chosen to approximate conditions in the foreshock region. Typically, density ratios are on the order of 10^{-2} - 10^{-3}. The small temperature ratios were chosen to approximate the steep positive slope of the electron beams. The steep positive slope is due to the time-of-flight mechanism. From Figure 8 one can see that if the beam temperature changes from $T_b/T_e = 0$ to $T_b/T_e = 0.1$, a downshift of plasma oscillations occurs if $0 < V_b/V_t \lesssim 3$. A change in the beam temperature may also occur simultaneously with a change in the beam velocity as the spacecraft penetrates deeper into the foreshock region. An indication of a change in the beam temperature is illustrated in Figure 4. From 1238:30 to 1239:00 UT, the contours of the reduced distribution at velocities less than 5000 km/sec shift more gradually as ISEE-1 penetrates more deeply into the foreshock region. The more gradual shift in the contours may be an indication that the steep positive slope of the time-of-flight distribution occurs near the foreshock boundary and becomes less steep as ISEE-1 moves into the foreshock region. Such a change in the steepness may increase the downshift of plasma oscillations from the plasma frequency.

Although the above numerical solutions to the linearized Vlasov equation are completely general, it is useful to solve the dispersion

relation analytically, by considering two limiting forms of Equation 5. By obtaining these solutions, the influence of various parts of the dispersion relation on the frequency of maximum growth can be illustrated. The limiting forms of Equation 5, for slightly different initial conditions, are discussed by Briggs [1964] and Grabbe [1984].

The first limiting form of Equation 5 can be obtained by assuming $V_b/V_t >> 1$. This limiting form is equivalent to the high phase velocity approximation, $\omega/k >> V_t$. Using the high phase velocity approximation for the plasma dispersion function (and in the limit of $\omega_i \to 0$), Equation 5 can be approximated as

$$D(k,\omega) = 0 \approx 1 - \frac{\omega_{pe}^2}{\omega^2} - \frac{3\,\omega_{pe}^4 (k\lambda_{De})^2}{\omega^4} - \frac{n_b/n_o (k\lambda_{De})^2}{(k\lambda_{De} V_b/V_t - \omega/\omega_{pe})^2} \quad , \quad (6)$$

where the additional assumption of a cold beam $T_b/T_e \to 0$ has been made. The third term in Equation 6 is a result of choosing a Maxwellian distribution for the electrons. By neglecting the third term, Equation 6 can be solved for small n_b/n_o using the weak beam approximation [Mikhailovskii, 1974]. Assuming $\omega_r = \omega_{pe} + \delta\omega$, one finds,

$$\omega_r \approx \omega_{pe}\left(1 - \frac{1}{2\sqrt[3]{2}}\, n_b/n_o^{1/3}\right) \quad . \quad (7)$$

Neglecting the fourth term in Equation 6 instead of the third term, one finds the solution to the resulting Equation is [Bohm and Gross, 1949]

$$\omega_r^2 \approx \omega_{pe}^2(1 + 3(k\lambda_{De})^2) \quad . \tag{8}$$

The curve illustrated in Figure 8 for values of $V_b/V_t > 3$ results from a combination effects illustrated by Equations 7 and 8. For $2 < V_b/V_t < 4$, $k\lambda_{De}$ is slightly less than one, so the approximation used to obtain Equation 8 is valid, resulting in $\omega_r > \omega_{pe}$. For $V_b/V_t > 4$, $k\lambda_{De}$ is much less than one, so the approximation used to obtain Equation 7 is valid resulting in $\omega_r < \omega_{pe}$. If the beam density becomes a significant fraction of the plasma density, one can see that $\omega_r << \omega_{pe}$ could result. This case is not considered because the typical beam densities in the foreshock region are very small compared to the plasma densities.

The second limiting form of Equation 5 is obtained by assuming $V_b/V_t << 1$. This limit is equivalent to the low phase velocity limit, $\omega_r/k << V_t$. For $\omega_r/k << V_t$ and $\omega_i \to 0$, $zZ(z) \approx 0$, so Equation 5 is approximated by,

$$D(k,\omega) = 0 \approx 1 + (k\lambda_{De})^2 - \frac{n_b/n_o(k\lambda_{De})^2}{(k\lambda_{De}V_b/V_t - \omega/\omega_{pe})^2} \tag{9}$$

where the additional assumption of a cold beam, $T_b/T_e \to 0$, has been made. Solving this equation for ω_r one finds,

$$\omega_r \approx \omega_{pe}\, k\lambda_{De} \left(V_b/V_t \pm \left(\frac{n_b/n_o}{1 + (k\lambda_{De})^2}\right)^{1/2}\right) \tag{10}$$

The general features of the curve in Figure 8 can be predicted using the approximations to the frequency of maximum growth in Equations 7, 8, and 10. From Equation 10 one can see that if $V_b/V_t \ll 1$ and $n_b/n_o \ll 1$, then $\omega_r/\omega_{pe} \ll 1$ and from Equation 8 one can see that if $V_b/V_t \approx 3$, then $\omega_r/\omega_{pe} \gtrsim 1$. Thus, the curve of ω_r/ω_{pe} versus V_b/V_t is predicted to vary smoothly from $\omega_r/\omega_{pe} \approx 0$ and $V_b/V_t \approx 0$ to $\omega_r/\omega_{pe} \gtrsim 1$ and $V_b/V_t \approx 3$. From Equation 7, one can see that if $V_b/V_t \gg 1$, then $\omega_r/\omega_{pe} \lesssim 1$. Thus, the curve of ω_r/ω_{pe} versus V_b/V_t is predicted to vary smoothly from $\omega_r/\omega_{pe} \gtrsim 1$ and $V_b/V_t \approx 3$ to $\omega_r/\omega_{pe} \lesssim 1$ and $V_b/V_t \gg 1$. The solutions in Equations 7, 8, and 10 are only approximate and are not valid when $V_b/V_t \approx 1$. When $V_b/V_t \approx 1$, one must solve the full dispersion relation (Equation 5) numerically as was done to obtain Figures 8 and 9.

COMPARISON OF THEORY TO OBSERVATIONS

In this section, the observations of plasma oscillations summarized at the end of Section II are compared to the predictions from the beam-plasma theory presented in Section III.

1. Plasma oscillations are observed at frequencies ranging from less than 0.1 f_{pe} to about 1.1 f_{pe}. In Figure 8, the observed frequency range is reproduced by an electron beam that varies in velocity from $V_b\ V_t >> 1$ to $V_b/V_t \approx 1$. The time-of-flight mechanism causes the beam velocity variation. When the spacecraft is near the foreshock boundary, only high velocity electrons reach the spacecraft, resulting in $V_b/V_t >> 1$. Far downstream of the foreshock boundary, electrons with velocities on the order of the electron thermal velocity reach the spacecraft, resulting in $V_b/V_t \approx 1$. Thus, the beam-plasma interaction and the time-of-flight mechanism combine to produce plasma oscillations in the observed frequency range.

2. As the plasma oscillations shift below the plasma frequency, their bandwidth increases from a few hundred hertz near the plasma frequency to ±2 kHz well below the plasma frequency. This increase in bandwidth may be produced by a small fluctuation in the beam velocity. A small fluctuation in the beam velocity could occur in the foreshock region because of changes in the magnetic geometry. The effect of a small fluctuation in the beam velocity is understood by considering Figure 8. For $V_b/V_t > 4$, the curve of ω_r/ω_{pe} versus V_b/V_t has near

zero slope. For a small fluctuation in the beam velocity, plasma oscillations are generated over a narrow range of frequencies centered near the plasma frequency. For $V_b/V_t \approx 1$, the curve of ω_r/ω_{pe} versus V_b/V_t has a large, positive slope. For a small fluctuation in the beam velocity, plasma oscillations are generated over a broad range of frequencies centered well below the plasma frequency.

The increase in the bandwidth as plasma oscillations shift below the plasma frequency may also be a consequence of the nature of the solutions of the dispersion relation. From Figure 8, it is concluded that when $V_b/V_t = 3$, plasma oscillations are narrow band emissions near the plasma frequency because the growth rate versus frequency is sharply peaked near the plasma frequency. When $V_b/V_t = 1$, plasma oscillations may occur over a broad range of frequencies because the growth rate varies by a small amount over a broad range of frequencies centered well below the plasma frequency. Thus, the change in bandwidth may be a consequence of the nature of the solutions to the dispersion relation or may be a result of a fluctuation in the beam velocity.

3. Plasma oscillations at the plasma frequency have wavelengths much greater than a Debye length. Plasma oscillations at frequencies well below the plasma frequency have wavelengths on the order of a few Debye lengths. The change in wavelength as plasma oscillations shift below the plasma frequency is illustrated in Figures 8 and 9. For $V_b/V_t \gg 1$, plasma oscillations occur near the plasma frequency and have long wavelengths, $(k\lambda_{De} \ll 1)$. As V_b/V_t decreases plasma oscillations shift first above, then below the plasma frequency and the wavelengths shift from $\lambda \gg \lambda_{De}$ to $\lambda \approx \lambda_{De}$. One can understand why the

wavelengths of plasma oscillations well below the plasma frequency are greater than the 30 meter electric antenna on ISEE-2 and less than the 215 meter electric antenna on ISEE-1 by considering some typical plasma parameters for the foreshock region. If one considers a typical electron temperature and number density of 1.5×10^5K and 9 cm^{-3}, respectively, then λ_{De} = 9 meters. If $2\pi\lambda_{De}$ is used as the criteria for the minimum wavelength in the plasma, then λ_{min} = 56 meters. This minimum wavelength is greater than the length of the 30 meter electric antenna on ISEE-2 but less than the length of the 215 meter antenna on ISEE-1. For λ = 215 meters, $k\lambda_{De}$ = 0.23. Referring to Figure 9, if $k\lambda_{De}$ = 0.23, then for $V_b/V_t < 4$, the wavelengths of plasma oscillations are less than 215 meters. When the spacecraft is located deep in the foreshock region, as in the example illustrated in Figure 3, $V_b/V_t < 4$ is satisfied, so the wavelengths are between 30 and 215 meters. One can see that the observed wavelengths of plasma oscillations at and below the plasma frequency are predicted using the beam-plasma theory.

In addition to being able to predict the short wavelength below the plasma frequency, the observations of short wavelengths above the plasma frequency reported by Etcheto and Faucheux [1984] are also predicted using the beam plasma theory in the previous section. Etcheto and Faucheux reported observations of wavelengths between 130 and 215 meters when ISEE-1 was a few R_E downstream of the foreshock boundary. Although they do not report a V_b/V_t ratio, one can see from Figure 8 that plasma oscillations above the plasma frequency occur for $2 \lesssim V_b/V_t \lesssim 5$. From Figure 9, $\lambda < 215$ m for $2 \lesssim V_b/V_t \lesssim 5$, thus both

the short wavelengths above and below the plasma frequency can be accounted for using the beam plasma theory.

4. Plasma oscillations much below the plasma frequency are correlated with times when ISEE-1 is located deep in the foreshock region, far downstream of the foreshock boundary. This correlation can be understood by considering Figure 5. When ISEE-1 is located near the foreshock boundary (case 1), V_b/V_t is much greater than one, resulting in plasma oscillations at the plasma frequency. When ISEE-1 is located deep in the foreshock region (case 2), V_b/V_t is approximately equal to one, resulting in plasma oscillations well below the plasma frequency.

The critical velocity can be computed using the equation, [Filbert and Kellogg, 1979]

$$V_c \approx \frac{D \cdot V_{sw}}{Diff} \qquad (11)$$

where V_c is the critical velocity, D is the distance from the tangent point to the spacecraft, Diff is the distance from the spacecraft to the tangent field line along the solar wind velocity direction, and V_{sw} is the solar wind velocity.

As an example, consider the event illustrated in Figure 4. The critical velocity for this event varies from $V_c \approx 2\ V_t$ at 1237:12 UT to $V_c \approx 0.8\ V_t$ at 1240:28 UT. Unfortunately, due to large uncertainties in the position and shape of the bow shock and the fact that 64 second averages of the magnetic field were used, these values of V_c are only rough estimates. Using these rough estimates for V_c and the graph in

Figure 8, one can predict that at 1237:12 UT plasma oscillations should occur near the plasma frequency and at 1240:28 UT plasma oscillations should occur well below the plasma frequency. From the middle panel in Figure 4, one can see that, as predicted, plasma oscillations occur at the plasma frequency at 1237:12 UT and plasma oscillations occur well below the plasma frequency at 1240:28 UT.

A better estimate of the critical velocity is obtained from Figure 6. In Figure 6 distribution A, the second peak in the reduced distribution occurs at $V_b \approx 9500$ km/sec, or $V_b \approx 6\ V_t$. From this value of V_b/V_t and from the graph in Figure 8, plasma oscillations are predicted at the plasma frequency. As seen in Figure 6, from 1237:51 to 1237:54 UT, plasma oscillations occur at the plasma frequency (~ 18 kHz). For Figure 6 distribution C, no peak is observed in the reduced distribution. However, the velocity where the distribution first deviates from the solar wind distribution may be taken as a lower limit on the critical velocity. As seen in distribution C, the lower limit is $V_c \approx 4000$ km/sec, or $V_c \approx 2\ V_t$. Using this value of V_c and the graph in Figure 8, plasma oscillations are predicted in the range of $0.8\ f_{pe} < f < 1.0\ f_{pe}$, depending on the beam temperature. Before comparing this prediction with the observations, the Doppler shift of the emissions must be considered. Using the value of $V_c \approx 2\ V_t$ and the graph in Figure 9, the value of $k\lambda_{De}$ ranges from 0.4 to 0.6, depending on the beam temperature. Using $k\lambda_{De} = 0.5$ and $\lambda_{De} = 9$ meters, $\lambda \approx 100$ meters. The solar wind velocity was 500 km/sec, so the maximum Doppler shift was approximately 5 kHz. In Figure 6 from 1238:27.6 to 1238:30.6 one can see that

the bursts of plasma oscillations occur at varying frequency averaging about 5 kHz below the plasma frequency. Thus, not only do the observations and predictions from the theory agree, this example verifies that the beam temperatures used in Figures 8 and 9 are reasonable estimates for the steep positive slopes of the beams that generate the plasma oscillations.

5. As the plasma oscillations shift below the plasma frequency, the flux of energetic electrons streaming from the bow shock increases at successively lower velocities. This correlation is interpreted as an indication that the time-of-flight mechanism discussed by Filbert and Kellogg is valid not only near the foreshock boundary, but is also valid far downstream of the foreshock boundary. Thus, plasma oscillations throughout the foreshock region are generated by a beam-plasma interaction.

Although the above evidence supports generation of plasma oscillations by a beam-plasma interaction, the apparent evolution of the reduced distribution from a double-peaked distribution to a single-peaked distribution as the spacecraft penetrates into the foreshock region is inconsistent with the beam-plasma theory presented in Section III. In the context of linear plasma theory, the single-peaked distribution observed downstream of the foreshock boundary does not have a free energy source capable of driving electron plasma oscillations. The fact that plasma oscillations are observed downstream of the foreshock boundary indicates that a beam must be present in the reduced distribution. Using a model distribution for an event similar to the one illustrated in Figure 6, it was found that the Goddard Spaceflight

Center Electron Spectrometer was capable of detecting a beam with any velocity, provided that the beam remained at a fixed velocity for the three seconds used to generate a reduced distribution. The observations of short duration bursts of plasma oscillations such as those illustrated in Figure 6 at 1238:20 - 1238:35 UT are an indication that downstream of the foreshock boundary, the generation of plasma oscillations occurs on much shorter time scales than 3 seconds. A typical burst lasts less than 50 milliseconds and has a bandwidth of 5 kHz. As pointed out above, a fluctuation in the beam velocity could account for the 5 kHz bandwidth of the bursts. Any 3-second time period may contain 20-40 bursts at varying frequencies. In the context of the beam-plasma theory in Section III, bursts of plasma oscillations at different frequencies are generated by bursts of electrons at different velocities. When averaged over 3 seconds, the bursts of electrons at different velocities would appear only as an enhancement in the flux of upstreaming electrons. Further study of the wave and particle data is needed to confirm evidence that temporal variations of an electron beam are the reason why reduced distributions far downstream of the foreshock boundary do not appear to have regions of positive slope (i.e., a well-defined beam). It is possible that thermal fluctuations or nonlinear effects may be found which can generate these waves without a requirement for a region of positive slope in the reduced distribution function. However, at present the linear beam-plasma instability presented in this paper is believed to be the most likely generation mechanism because the predictions from this mechanism agree with the observed characteristics of plasma oscillations in the foreshock region.

ACKNOWLEDGEMENTS

The authors thank C. S. Lin for providing routines used to approximate the plasma dispersion function and to solve the linear dispersion relation.

The research at the University of Iowa was supported by contract NAS5-26819 with Goddard Space Flight Center, grant NGL-16-001-043 with NASA Headquarters, and grant N00014-76-C-0016 with the Office of Naval Research.

REFERENCES

Anderson, K. A., Energetic electrons of terrestrial origin upstream in the solar wind, J. Geophys. Res., 73, 2387, 1968.

Anderson, K. A., Energetic electrons of terrestrial origin behind the bow shock and upstream in the solar wind, J. Geophys. Res., 74, 95, 1969.

Anderson, R. R., G. K. Parks, T. E. Eastman, D. A. Gurnett, and L. A. Frank, Plasma waves associated with energetic particles streaming into the solar wind from the Earth's bow shock, J. Geophys. Res., 86, 4493, 1981.

Bohm, D., and E. P. Gross, Theory of plasma oscillations. A. Origin of medium-like behavior, Phys. Rev., 75, 1851, 1949.

Briggs, Richard J., Electron-stream interaction with plasmas, M.I.T. Press, Cambridge, MA, 1964.

Etcheto, J., and M. Faucheux, Detailed study of electron plasma waves upstream of the Earth's bow shock, J. Geophys. Res., in press, 1984.

Feldman, W. C., J. R. Asbridge, S. J. Bame, M. D. Montgomery, and S. P. Gary, Solar wind electrons, J. Geophys. Res., 80, 4181, 1975.

Filbert, P. C., and P. J. Kellogg, Electrostatic noise at the plasma frequency beyond the Earth's bow shock, J. Geophys. Res., 84, 1369, 1979.

Fitzenreiter, R. J., A. J. Klimas, and J. D. Scudder, Detection of bump-on-tail reduced electron velocity distributions at the electron foreshock boundary, Geophys. Res. Lett., 11, 496, 1984.

Fredricks, R. W., C. F. Kennel, F. L. Scarf, G. M. Crook, and I. M. Green, Detection of electric-field turbulence in the Earth's bow shock, Phys. Rev. Lett., 21, 1761, 1968.

Fredricks, R. W., F. L. Scarf, and L. A. Frank, Nonthermal electrons and high-frequency waves in the upstream solar wind. 2. Analysis and interpretation, J. Geophys. Res., 76, 6691, 1971.

Fredricks, R. W., F. L. Scarf, C. T. Russell, and M. Neugebauer, Detection of solar-wind electron plasma frequency fluctuations in an oblique nonlinear magnetohydrodynamic wave, J. Geophys. Res. Lett., 77, 3598, 1972.

Grabbe, C. L., A model for chorus associated electrostatic bursts, J. Geophys. Res., 89, 919, 1984.

Gurnett, D. A., R. R. Anderson, F. L. Scarf, R. W. Fredricks, E. J. Smith, Initial results from the ISEE-1 and -2 plasma wave investigation, Space Sci. Rev., 23, 103, 1979.

Gurnett, D. A., and L. A. Frank, Electron plasma oscillations associated with Type III radio emissions and solar electrons, Solar Phys., 45, 477, 1975.

Gurnett, D. A., F. L. Scarf, R. W. Fredricks, E. J. Smith, The ISEE-1 and ISEE-2 plasma wave investigation, IEEE Trans. Geosci. Electr., GE-16, 225, 1978.

Harvey, C. C., J. Etcheto, Y. de Javel, R. Manning, and M. Petit, The ISEE electron density experiment, IEEE Trans. Geosci. Electr., GE-16, 231, 1978.

Hoang, S., J. L. Steinberg, G. Epstein, P. Tilloles, J. Fainberg, and R. G. Stone, The low-frequency continuum as observed in the solar wind from ISEE-3: Thermal electrostatic noise, J. Geophys. Res., 85, 3419, 1980.

Klimas, A. J., A mechanism for plasma waves at the harmonics of the plasma frequency in the electron foreshock boundary, J. Geophys. Res., 88, 9081, 1983.

Mikhailovskii, A. B., Theory of Plasma Instabilities (Vol. 1: Instabilities of a Homogeneous Plasma), Consultants Bureau, New York-London, 1974.

Muller, D. E., A method for solving algebraic equations using an automatic computer, Math. Comp., 10, 208, 1956.

Ogilvie, K. W., J. D. Scudder, and H. Doong, The electron spectrometer experiment on ISEE-1, IEEE Trans. Geosci. Electr., GE-16, 261, 1978.

Reinleitner, L. A., D. A. Gurnett, T. E. Eastman, Electrostatic bursts generated by electrons in Landau resonance with whistler mode chorus, J. Geophys. Res., 88, 3079, 1983.

Rodriguez, P., and D. A. Gurnett, Electrostatic and electromagnetic turbulence associated with the Earth's bow shock, J. Geophys. Res., 80, 19, 1975.

Rodriguez, P., and D. A. Gurnett, Correlation of bow shock plasma wave turbulence with solar wind parameters, J. Geophys. Res., 81, 2871, 1976.

Scarf, F. L., R. W. Fredricks, L. A. Frank, and M. Neugebauer, Nonthermal electrons and high-frequency waves in the upstream solar wind. 1. Observations, J. Geophys. Res., 76, 5162, 1971.

Scarf, F. L., R. W. Fredricks, L. A. Frank, C. T. Russell, P. J. Coleman, Jr., and M. Neugebauer, Direct correlations of large amplitude waves with suprathermal protons in the upstream solar wind, J. Geophys. Res., 75, 7316, 1970.

FIGURE CAPTIONS

Figure 1 Electrons streaming from the bow shock are convected downstream due to the motion of the solar wind. Electrons originating from the tangent point with very high energies define a boundary called the electron foreshock boundary. Downstream of this boundary is a region called the electron foreshock region. In this region the "beam" of electrons originating from the bow shock has a characteristic lower cutoff velocity. This cutoff velocity occurs because electrons below a certain critical velocity are convected downstream before they reach the spacecraft.

Figure 2 The upper panel is a frequency-time wideband spectrogram from the ISEE-1 wideband receiver taken when the spacecraft was located in the foreshock region. The lower panel is a plot of the plasma frequency determined from electron density measurements. From 0633 to 0633:30 UT and from 0638:30 to 0639 UT, plasma oscillations are observed to shift well below the plasma frequency. Coincident with these shifts is an increase in the bandwidth of the emissions from a few

hundred Hz at the plasma frequency to ±2 kHz well below the plasma frequency.

Figure 3 A plot of a 20-minute average spectral density versus frequency, for an event when plasma oscillations occurred well below the plasma frequency. The plasma frequency for this event was about 30 kHz. For frequencies between 10 and 20 kHz, the spectral density from ISEE-2 is greater than that from ISEE-1 by about a factor of 5. This difference indicates that the wavelengths of the plasma oscillations well below the plasma frequency are shorter than the ISEE-1 antenna (215 meters) and longer than the ISEE-2 antenna (30 meters).

Figure 4 The upper panel is a plot of iso-contours of $-\ell n(F(v_{\parallel}))$ for electrons streaming from the bow shock. A shift of a contour from low to high velocities is an indication of an increase in the flux of electrons at low velocities. The middle panel is a frequency-time spectrogram. The narrowband emissions at 18 kHz are electron plasma oscillations. The lower panel is a plot of Diff. A large, negative value of Diff implies that ISEE-1 is far downstream of the foreshock boundary. From 1237 to 1239 UT, ISEE-1 penetrates deeply into the foreshock region, the flux of electrons streaming from

the bow shock increases at successively lower velocities, and plasma oscillations shift first above, then below the plasma frequency. The reverse happens from 1240 to 1242 UT.

Figure 5 The reduced one-dimensional distribution depends on the spacecraft location in the foreshock region. When the spacecraft is located far downstream the foreshock boundary (case 1), the critical velocity is on the order of the electron thermal velocity. When the spacecraft is located near the foreshock boundary, (case 2), the critical velocity is much greater than the electron thermal velocity.

Figure 6 In the upper panels, three reduced one-dimensional distribution obtained from 3 seconds of data spaced 18 seconds apart are illustrated. The middle panel is a plot of high resolution wideband data. The lower panel is a plot of Diff. At 1237:51 - 1237:54 UT, a second peak is observed in the reduced distribution. At 1238:09.2 - 1238:12.2 UT, a plateau is observed in the reduced distribution. At 1238:27.6 - 1238:30.6 UT when ISEE-1 is about 25 R_E downstream of the foreshock boundary, no beam is visible in the reduced distribution. One reason why no beam is visible may be that the beam is varying in velocity space much faster than

the 3 seconds used to generate the distribution. Observations of short duration bursts of plasma oscillations at varying frequencies may be evidence of temporal variation of the beam.

Figure 7 Solutions to the linear dispersion relation $D(k,\omega) = 0$ are illustrated. The growth rate or imaginary part of the frequency is plotted versus the real part of the frequency. The number density ratio and beam temperature ratio were fixed at 0.01 and 0.0, respectively. Curves representing $\omega(k)$ for various values of V_b/V_t are illustrated. For specific values of V_b/V_t and n_b/n_o, the observed frequency will be the frequency with the maximum growth rate.

Figure 8 The frequency of maximum growth determined from solutions of $D(k,\omega) = 0$ is plotted versus V_b/V_t. The number density ratio was fixed at 0.01. Curves for various values of T_b/T_o are illustrated. For $2 < V_b/V_t < 5$, plasma oscillations occur above the plasma frequency. For $V_b/V_t < 2$, plasma oscillations occur below the plasma frequency.

Figure 9 The wave number of maximum growth is plotted versus V_b/V_t. The number density ratio was fixed at 0.01. As V_b/V_t decreases, wavelengths of plasma oscillations decrease. For $V_b/V_t \lesssim 4.5$ wavelengths of plasma oscillations are less than the 215 meter antenna on ISEE-1.

A-G84-80-1

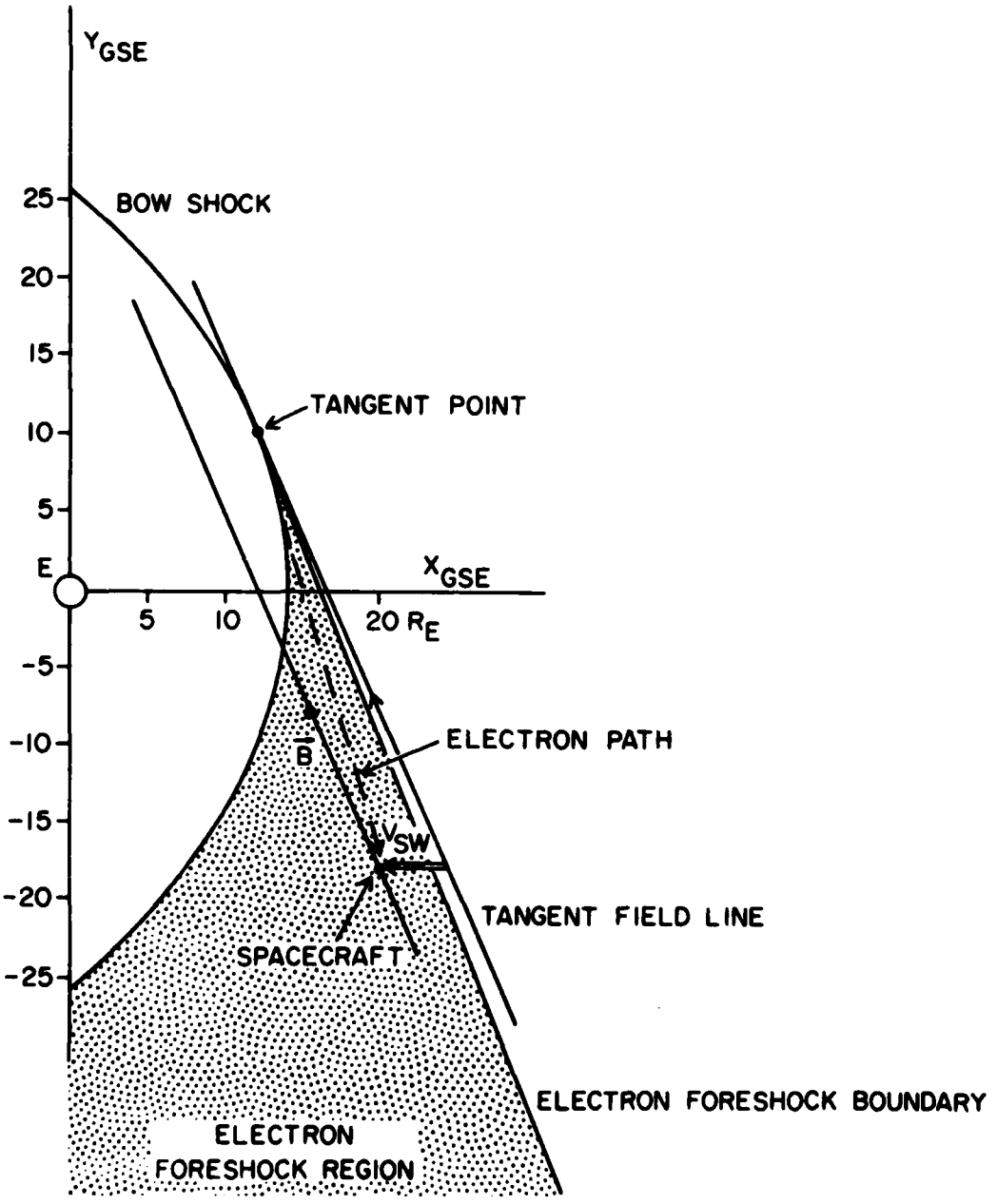

Figure 1

C-G84-110-3

ISEE-1 WIDEBAND DATA
OCTOBER 31, 1977 DAY 304
R = 22 R_E LOCAL TIME = 11 HRS

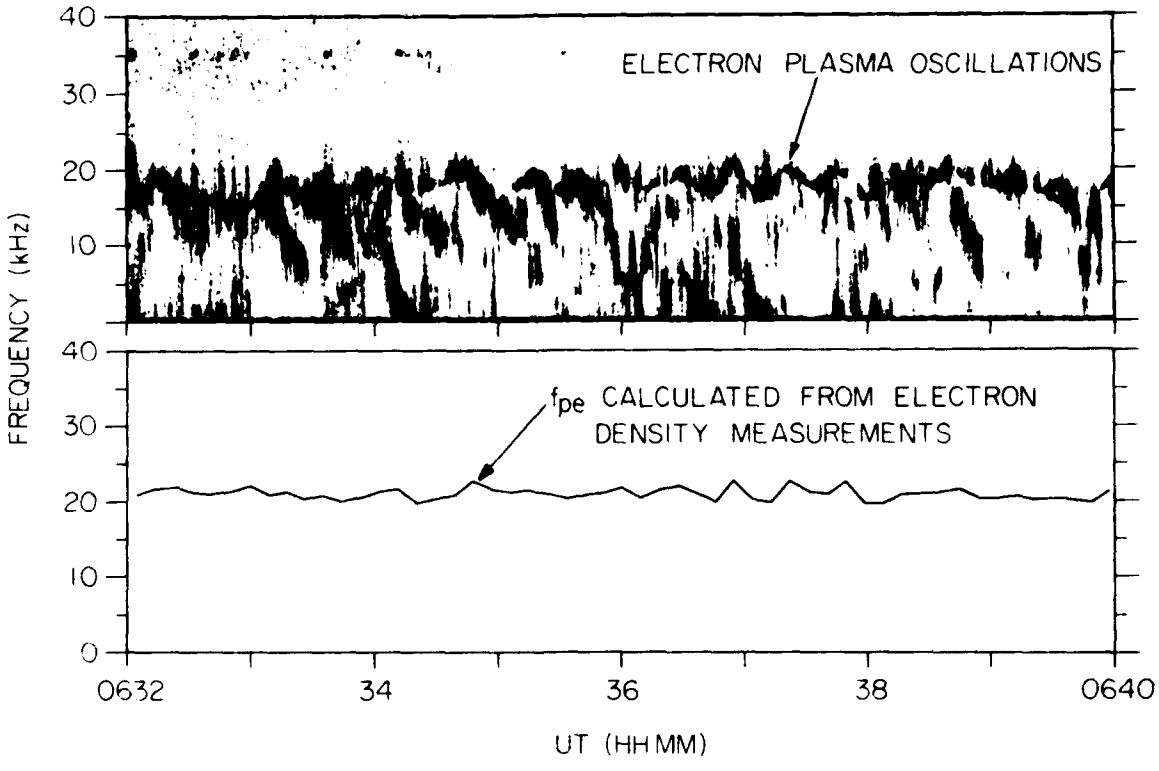

Figure 2

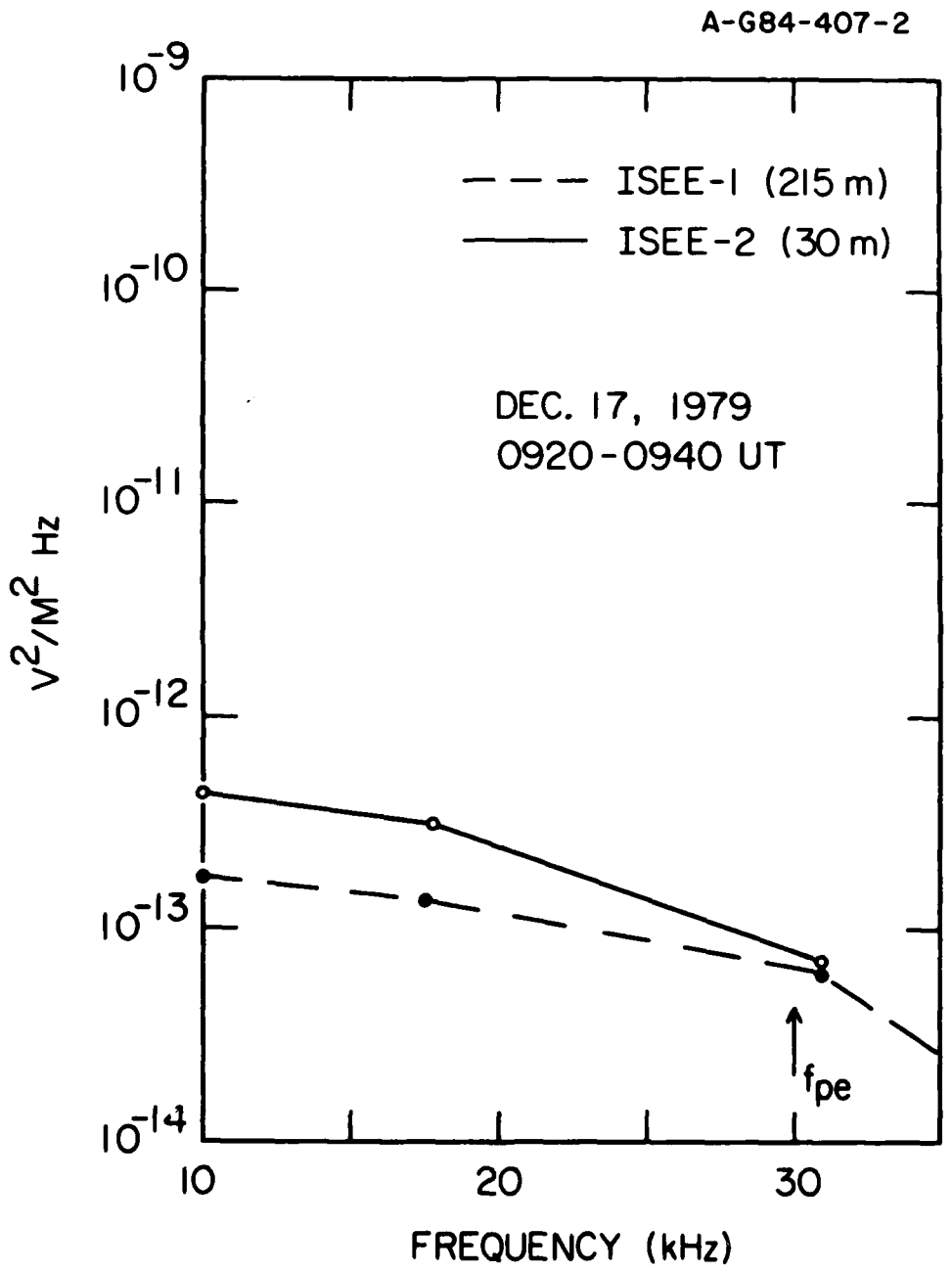
A-G84-407-2
ISEE-1 (215 m)
ISEE-2 (30 m)
DEC. 17, 1979
0920-0940 UT
10^{-9}
10^{-10}
10^{-11}
10^{-12}
10^{-13}
10^{-14}
V^2/M^2 Hz
f_{pe}
10
20
30
FREQUENCY (kHz)

Figure 3

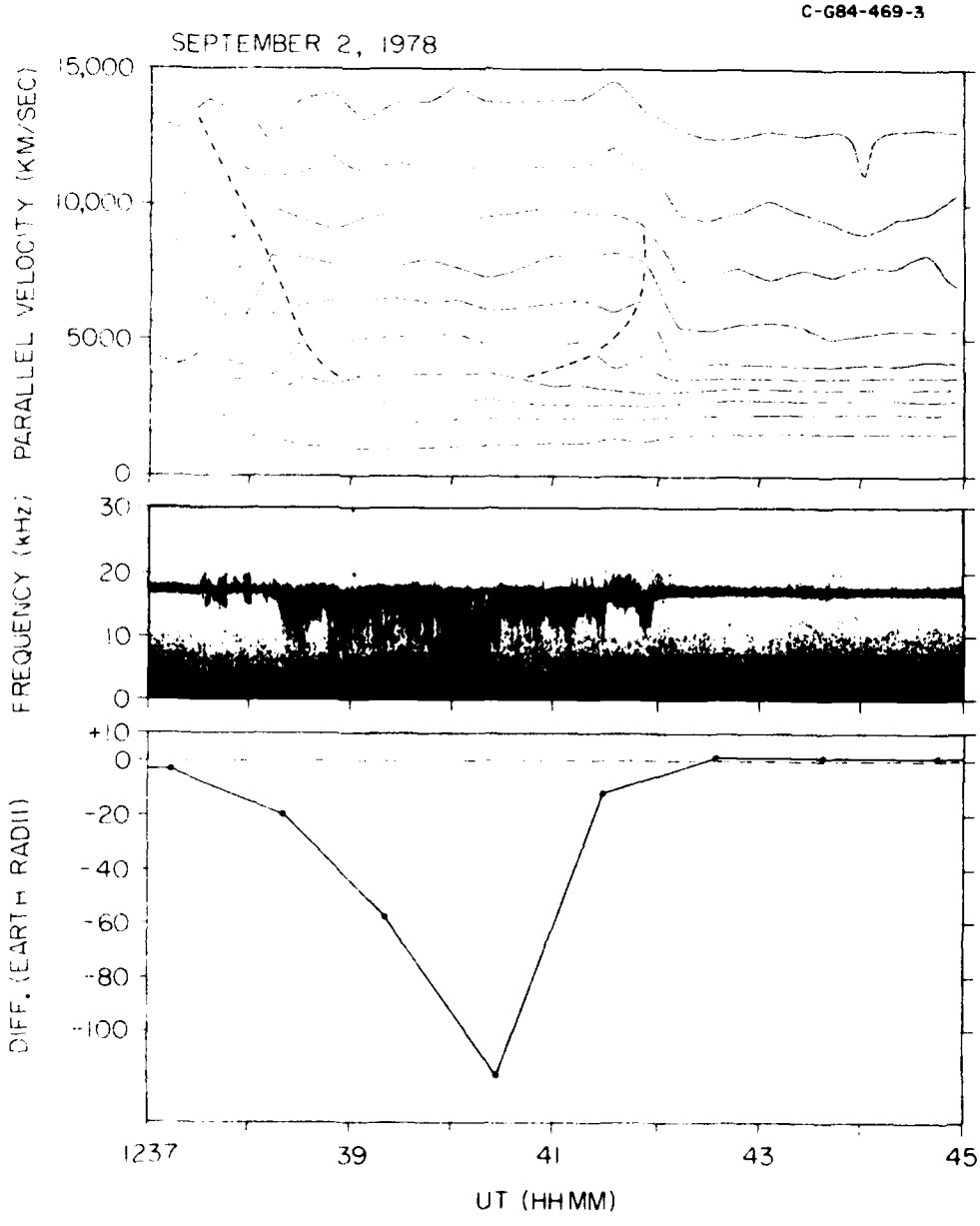
C-G84-469-3
SEPTEMBER 2, 1978
PARALLEL VELOCITY (KM/SEC)
15,000
10,000
5000
0
FREQUENCY (kHz)
30
20
10
0
DIFF. (EARTH RADII)
+10
0
-20
-40
-60
-80
-100
1237
39
41
43
45
UT (HHMM)

Figure 4

A-G84-408

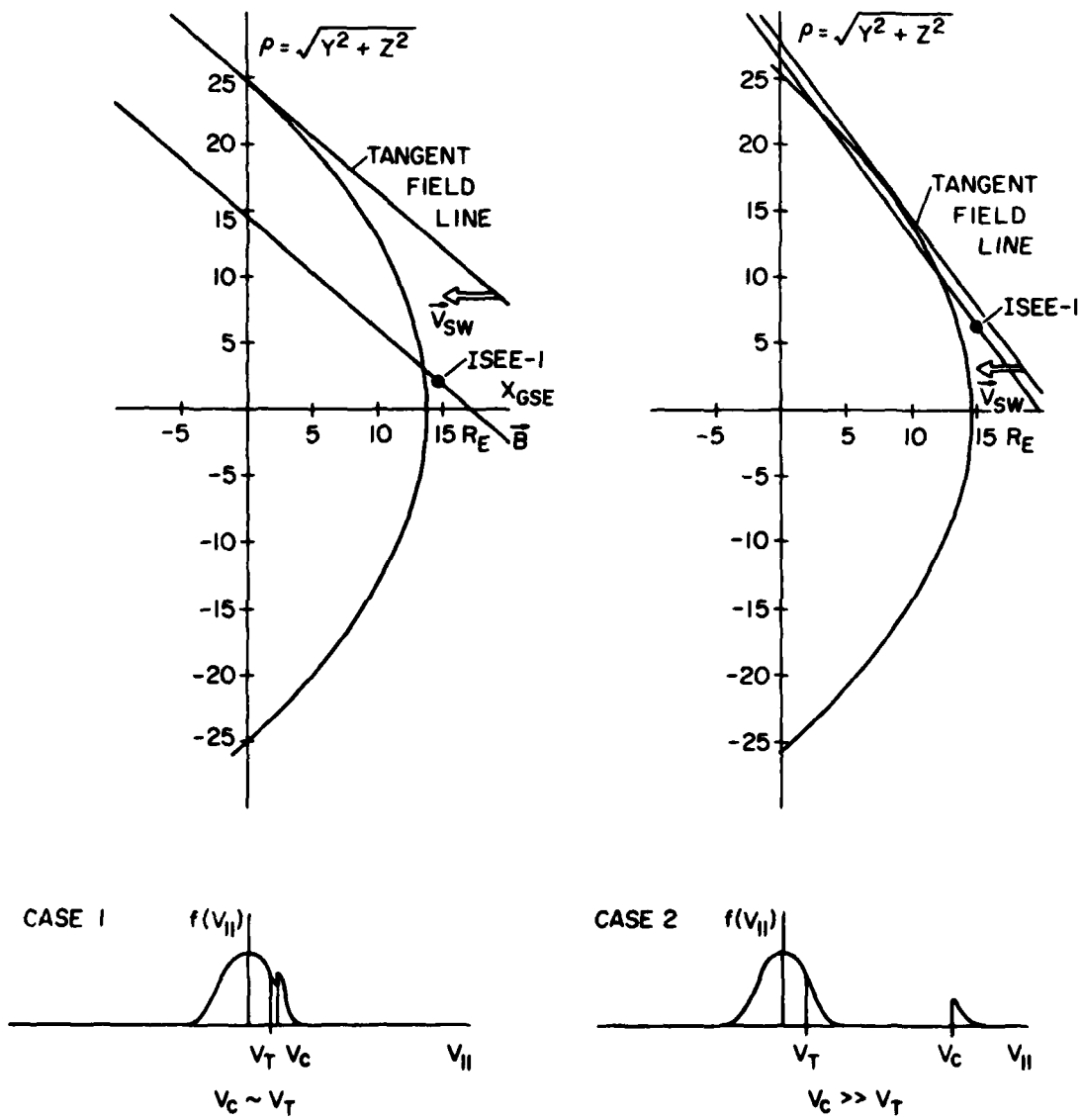

Figure 5

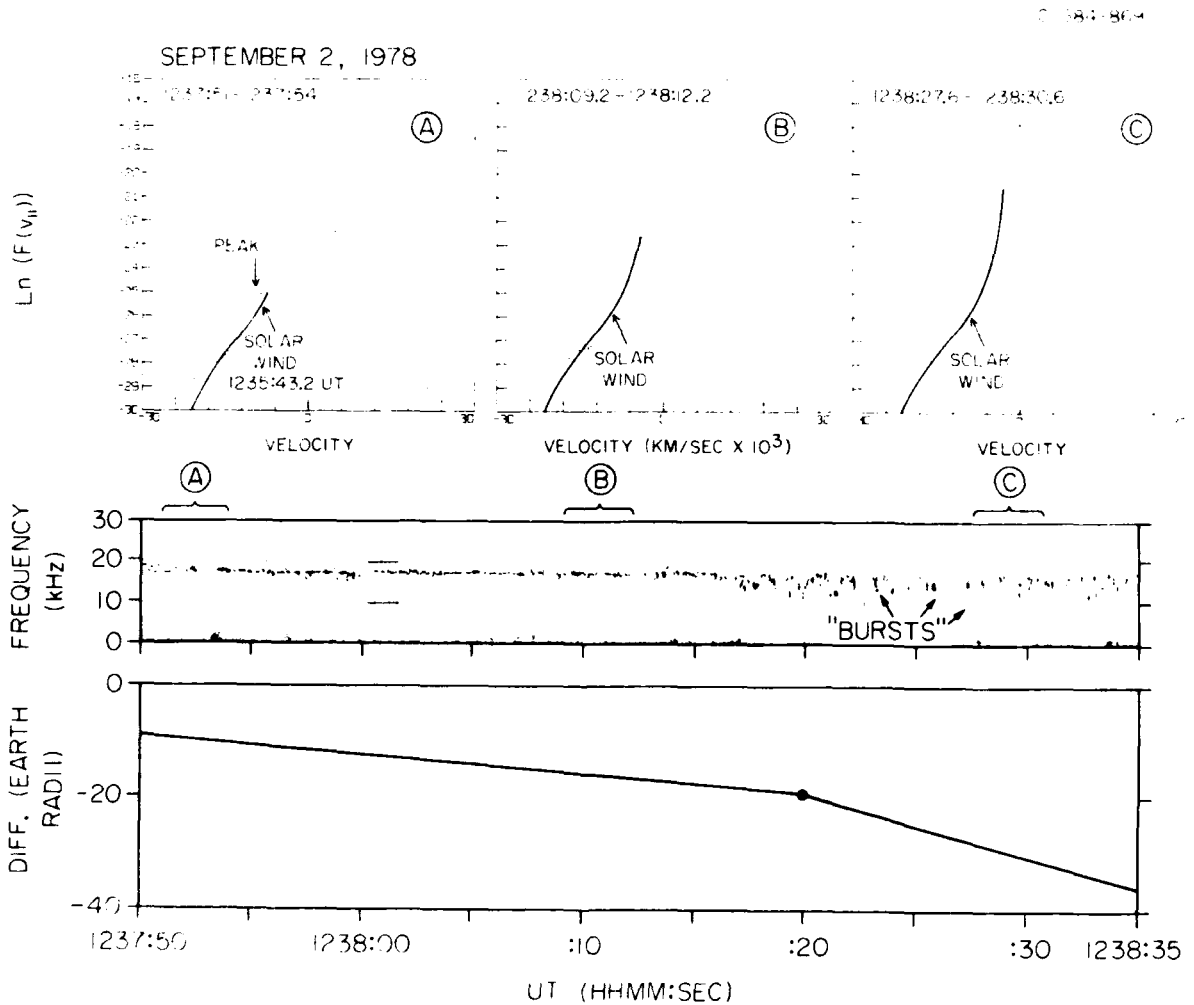
SEPTEMBER 2, 1978
1238:09.2 - 1248:12.2
1238:27.6 - 1238:30.6
A
B
C
PEAK
SOLAR WIND
1235:43.2 UT
SOLAR WIND
SOLAR WIND
Ln (F(v_II))
VELOCITY
VELOCITY (KM/SEC X 10^3)
VELOCITY
FREQUENCY (kHz)
30
20
10
0
"BURSTS"
DIFF. (EARTH RADII)
0
-20
-40
1237:50
1238:00
:10
:20
:30
1238:35
UT (HHMM:SEC)

Figure 6

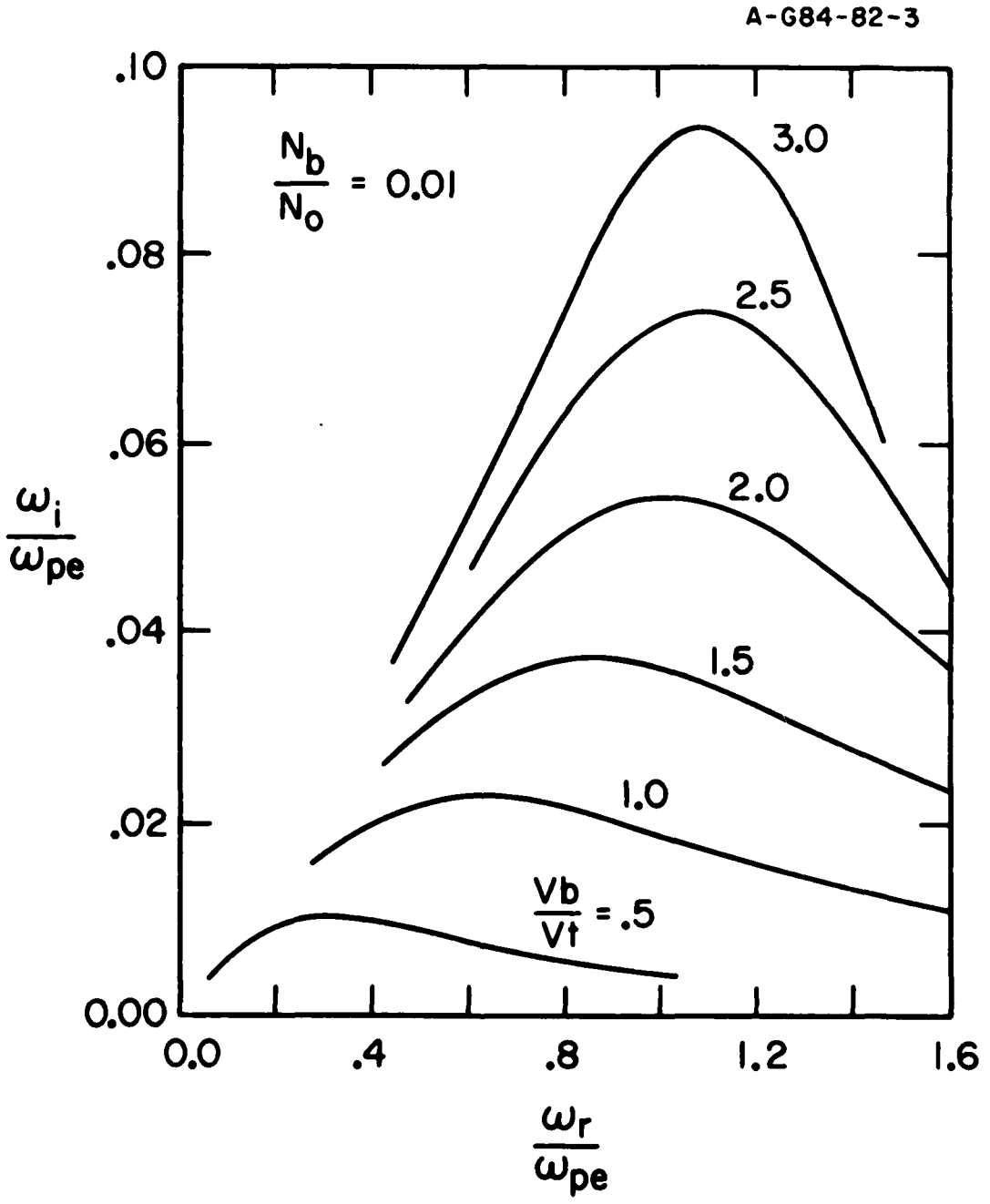
A-G84-82-3
.10
.08
.06
.04
.02
0.00
$\frac{N_b}{N_o}$ = 0.01
3.0
2.5
2.0
1.5
1.0
$\frac{Vb}{Vt}$ = .5
$\frac{\omega_i}{\omega_{pe}}$
0.0
.4
.8
1.2
1.6
$\frac{\omega_r}{\omega_{pe}}$

Figure 7

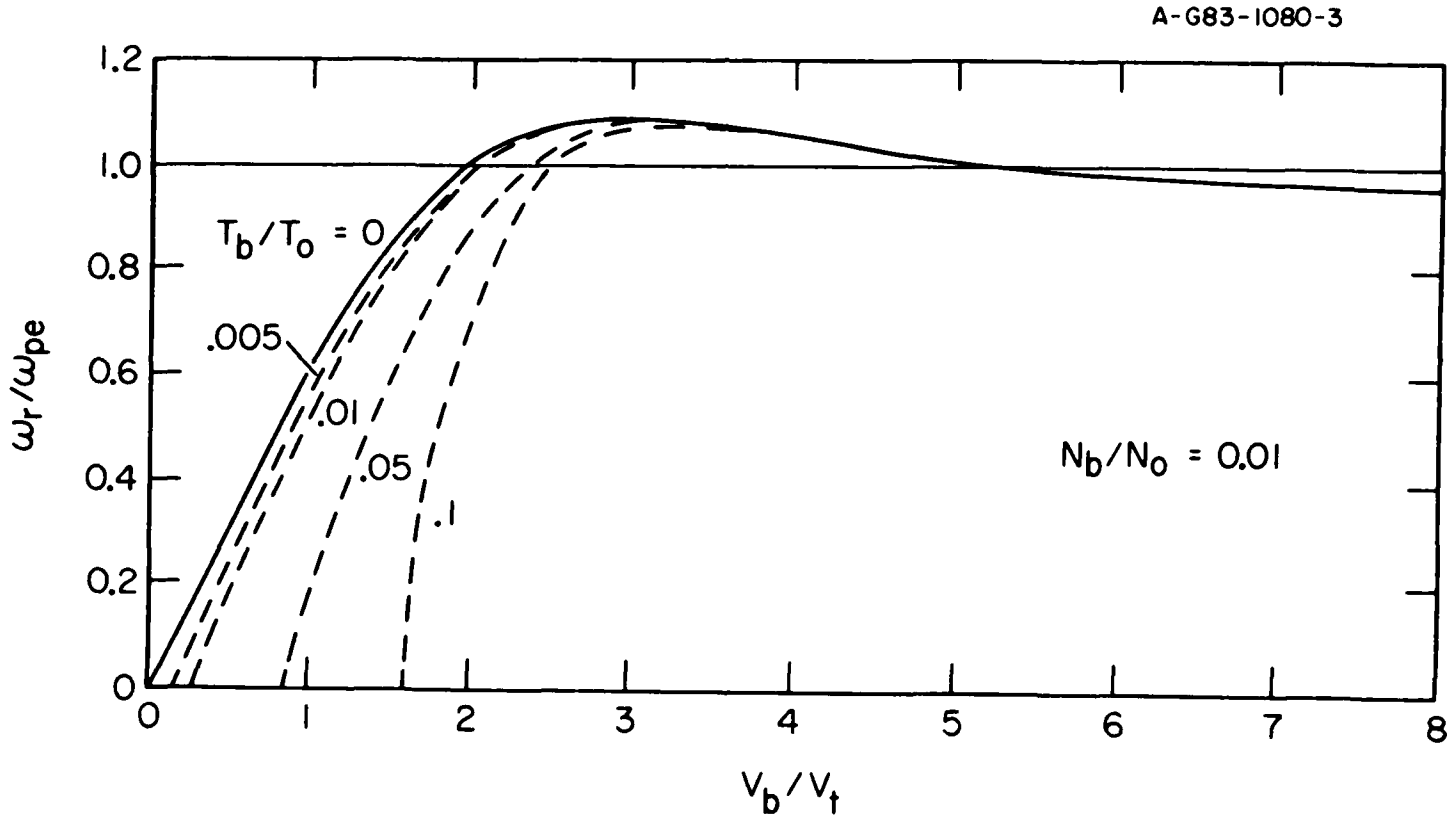
A-G83-1080-3
1.2
1.0
0.8
0.6
0.4
0.2
0
ω_r/ω_{pe}
$T_b/T_o = 0$
.005
.01
.05
.1
$N_b/N_o = 0.01$
0
1
2
3
4
5
6
7
8
V_b/V_t

Figure 8

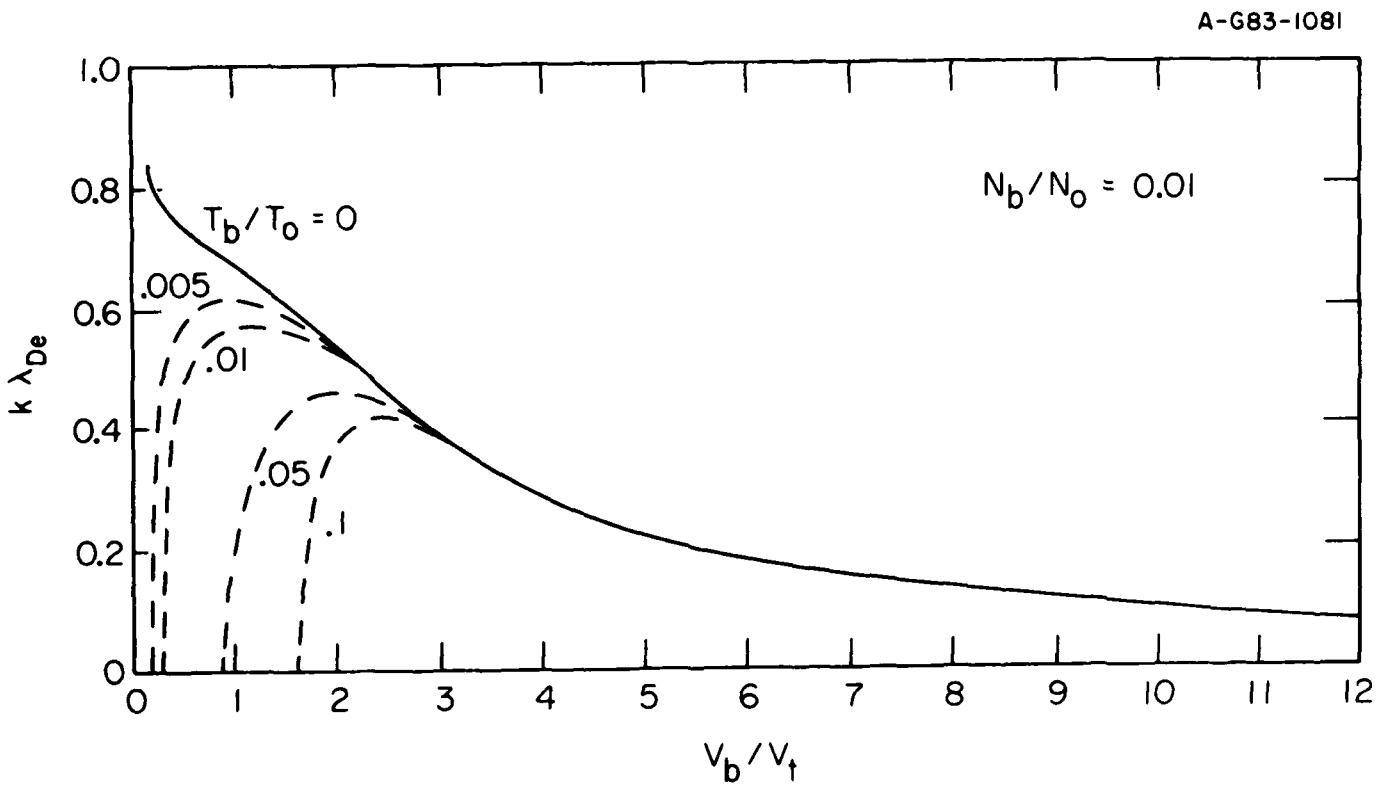
A-G83-1081
1.0
0.8
0.6
0.4
0.2
0
k λDe
Tb/To = 0
.005
.01
.05
.1
Nb/No = 0.01
0
1
2
3
4
5
6
7
8
9
10
11
12
Vb/Vt

Figure 9

END

FILMED

4-85

DTIC